

RESEARCH ARTICLE | APRIL 03 2023

# Electromechanical resonances and field-emission-induced self-oscillations of single crystal diamond needles

Victor I. Kleshch ; Rinat R. Ismagilov; Vsevolod V. Mukhin; ... et. al

 Check for updates

*Appl. Phys. Lett.* 122, 144101 (2023)

<https://doi.org/10.1063/5.0138141>

  
View  
Online

  
Export  
Citation

CrossMark

## Articles You May Be Interested In

Magnetic needle rheometer

*Rev Sci Instrum* (September 1989)

Influence of needle impact velocity on the jetting effect of a piezoelectric needle-collision jetting dispenser

*AIP Advances* (April 2019)

Phonograph Needle Drag Distortion

*J Acoust Soc Am* (June 2005)



 CryoComplete

A total solution for low-temperature characterization

[Learn more >](#)



# Electromechanical resonances and field-emission-induced self-oscillations of single crystal diamond needles

Cite as: Appl. Phys. Lett. **122**, 144101 (2023); doi: [10.1063/5.0138141](https://doi.org/10.1063/5.0138141)

Submitted: 8 December 2022 · Accepted: 24 March 2023 ·

Published Online: 3 April 2023








View Online



Export Citation



CrossMark

Victor I. Kleshch,<sup>1,a)</sup>  Rinat R. Ismagilov,<sup>1</sup>  Vsevolod V. Mukhin,<sup>1</sup> Anton S. Orekhov,<sup>2</sup>  Philippe Poncharal,<sup>3</sup>   
Stephen T. Purcell,<sup>3</sup> and Alexander N. Obraztsov<sup>1</sup> 

## AFFILIATIONS

<sup>1</sup>Department of Physics, Lomonosov Moscow State University, Moscow 119991, Russia

<sup>2</sup>Shubnikov Institute of Crystallography of FSRC “Crystallography and Photonics” of the Russian Academy of Sciences, Moscow 119333, Russia

<sup>3</sup>Institut Lumière Matière, Université Lyon 1, CNRS, UMR 5306, F-69622 Villeurbanne Cedex, France

<sup>a)</sup> Author to whom correspondence should be addressed: [klesch@polly.phys.msu.ru](mailto:klesch@polly.phys.msu.ru)

## ABSTRACT

Due to its outstanding mechanical characteristics, diamond is an ideal material for use in micro- and nano-electromechanical systems. In this paper, we report on the investigation of vibrational properties of singly clamped needlelike diamond microcrystallites with nanoscale tips. The single-crystal diamond needles were produced by selective oxidation of polycrystalline films grown using chemical vapor deposition. The study of resonant oscillations driven by the AC voltage indicated that the elastic modulus of such diamond needles is close to that of bulk single crystal diamond. A self-oscillation regime induced by the DC voltage during field emission from the apex of a diamond needle is also demonstrated. It is shown that this regime can be used for efficient DC–AC conversion in microdevices. The high structural quality of diamond needles, their remarkable mechanical properties, and the relative ease of their mass fabrication make them promising candidates for application in various electromechanical systems, field-emission devices, and scanning probe techniques.

Published under an exclusive license by AIP Publishing. <https://doi.org/10.1063/5.0138141>

The high values of the elastic modulus, thermal conductivity, and hardness and the low intrinsic mechanical losses make diamond an ideal material for creating electromechanical resonators for sensors and precision measurements.<sup>1–4</sup> The most advanced resonators are based on single-crystal diamond and produced by top-down methods from bulk diamond substrates.<sup>5–7</sup> At the same time, the recently demonstrated bottom-up fabrication of high-aspect-ratio single-crystal diamond microcrystallites<sup>8,9</sup> may be a promising alternative to the top-down state-of-the-art fabrication techniques.

Resonators capable of generating AC signals are of particular interest for various microelectromechanical systems (MEMS). A variant of such a resonator in the form of a singly clamped nanowire that generates alternating voltage by mechanical self-oscillation initiated due to field electron emission driven by the DC voltage was proposed in Ref. 10. To date, such self-oscillations have been demonstrated for field emitters based on silicon carbide (SiC) nanowires<sup>10,11</sup> and carbon nanotubes.<sup>12–15</sup> Given the outstanding mechanical properties of diamond, realization of a self-oscillation regime in a system with a field

emitter based on single-crystal diamond can potentially lead to a significant improvement in the characteristics of such micromechanical DC–AC converters.

In this work, we study the mechanical properties of the resonators based on single-crystal diamond micro-needles. Using the dynamic resonance method,<sup>16</sup> we investigate their natural frequencies, quality factors, and elastic modulus. Since such needles demonstrate efficient field emission,<sup>17,18</sup> we also explore the possibility of realization of the self-oscillation regime.

Single-crystal diamond needles were fabricated by direct current discharge plasma enhanced chemical vapor deposition (CVD) of a polycrystalline diamond film and its subsequent selective oxidation.<sup>8,9,19</sup> Hydrogen and methane gas mixture was used in the CVD process. The substrate temperature was 900 °C. The growth rate of the diamond film was about 1 μm per hour. After growth, the film was oxidized for 20 h by heating in air at normal atmospheric pressure and a temperature of 600 °C. As a result of oxidation, the less ordered component of the film was removed due to its gasification and individual

needlelike diamond microcrystals remained on the substrate. In a single bottom-up process, several million needles are produced [Fig. 1(a)]. The needles have a shape close to a pyramid with a rectangular base. The pyramid base coincides with the (100) diamond facet. By changing the deposition parameters, it is possible to vary not only the size of the needles, but also the dimension of the cross section [see examples in Figs. 1(b)–1(e)], which is important for production of resonators with desired properties.

We used two different setups based on transmission and scanning electron microscopes (TEM and SEM) in which it was possible to measure electromechanical resonance and emission-induced self-oscillations, respectively. The resonant forced oscillations of the diamond needles were studied inside a TOPCON EM002b TEM at a vacuum level of  $\sim 10^{-7}$  Torr, similar to that described in Refs. 20 and 21. Each needle was fixed on a sharpened tungsten wire, which was mounted in a TEM sample holder. During measurements, the needle tip was located at a distance of  $\sim 1$  mm from a gold ball of 1 mm in diameter [Fig. 2(a)]. DC voltage  $V_{DC}$  was applied to the needle holder, and a sinusoidal excitation voltage with an amplitude of up to 10 V was applied to the golden ball. The amplitude of resonant oscillations was determined from TEM images.

The field emission properties and self-oscillations of diamond needles under action of a DC voltage were measured inside FEI Versa 3D SEM chamber at a vacuum level of  $\sim 10^{-6}$  Torr. In this case, a

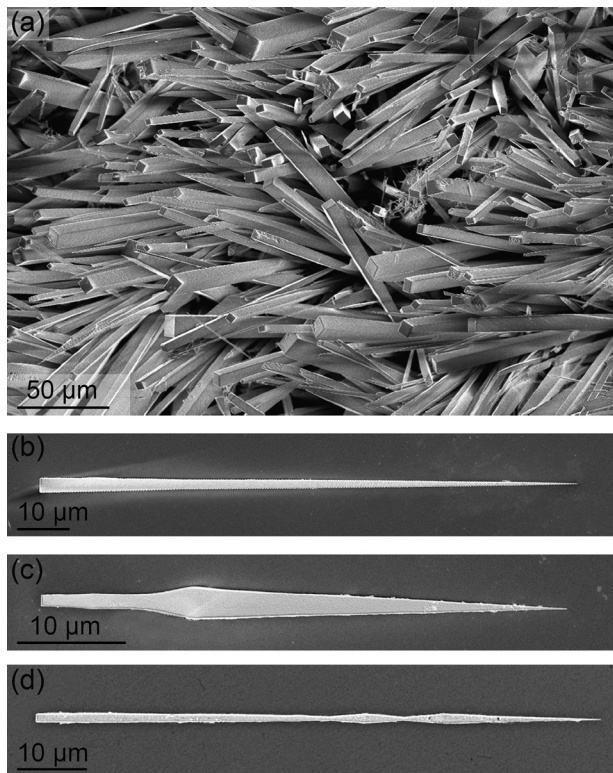


**FIG. 1.** (a) Scanning electron microscopy images of diamond needles after their extraction from a CVD-grown polycrystalline diamond film treated by selective oxidation. (b)–(d) SEM images of individual diamond needles obtained in the CVD processes with different and variable parameters.

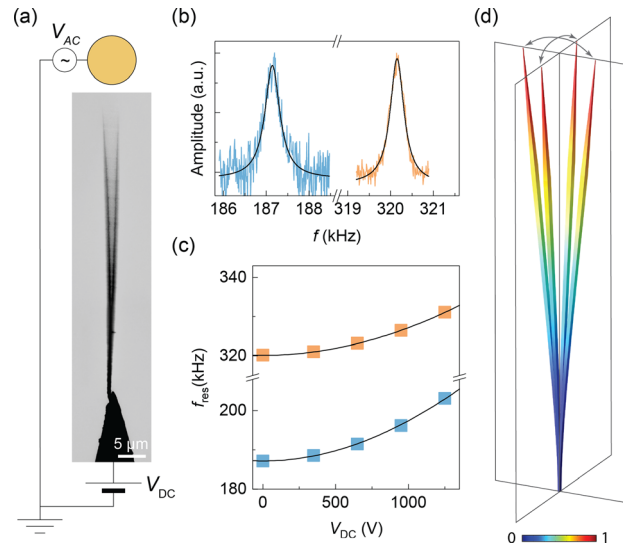


**FIG. 2.** (a) TEM image of vibrating diamond needle and the measurement scheme used for the study of the resonant oscillations. (b) Oscillation amplitude vs frequency of the excitation voltage at  $V_{DC} = 0$  V. Black lines are Lorentz fits. (c) Resonance frequency vs applied DC voltage. Black lines are fits using  $f_{res}^2(V_{DC}) - f_{res}^2(V_{DC} = 0) \sim V_{DC}^2$  equation. (d) Deformation of the needle for two polarizations of the first eigenmode. The colormap shows the relative displacement of the needle points from the equilibrium position.

sharpened tungsten wire was used as an anode. It was located near the diamond needle tip [Fig. 3(a)]. DC voltage was applied between the needle holder and the anode. The field emission current was measured using a Keithley 6487 picoammeter. Microscopic images were

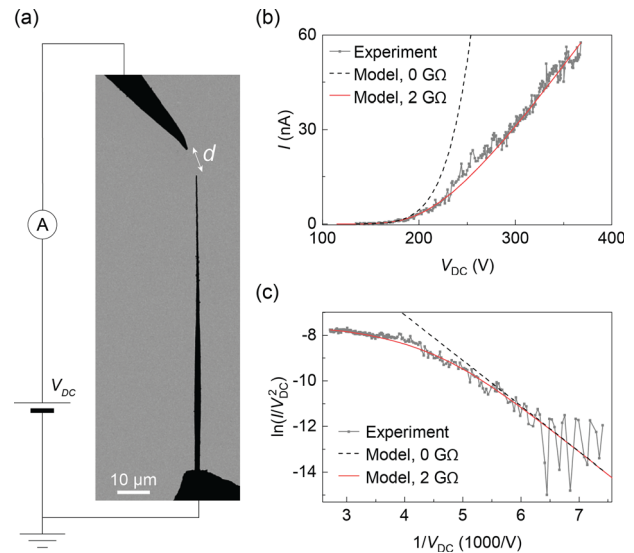


**FIG. 3.** (a) STEM image of a diamond needle at the anode–cathode distance  $d = 8 \mu\text{m}$  and scheme of field emission measurements. (b) Field emission current–voltage characteristic. Dashed and solid lines are fits using Eq. (1) at  $a = 2.5 \times 10^{-9} \text{ AN}^2$ ,  $b = 2000 \text{ V}$ ,  $R = 0 \text{ G}\Omega$ , and  $R = 2 \text{ G}\Omega$ , correspondingly. (c) FN plot for the current–voltage curves shown in panel (b).

obtained using a solid-state scanning transmission electron microscopy (STEM) detector.

The needles investigated in this work had lengths in the range from 50 to 100  $\mu\text{m}$ . The study of resonant vibrations has shown that their fundamental frequencies lie in the range from 100 kHz to several MHz depending on the specific shape and dimensions. It should be noted that a similar range of frequencies is also observed for diamond cantilevers of similar sizes fabricated by the top-down method.<sup>7</sup> Figure 2(b) shows a typical dependence of the oscillation amplitude on the frequency of the excitation voltage for the needle shown in Fig. 2(a). Two Lorentz peaks are observed at frequencies  $f_1 = 320.2$  kHz and  $f_2 = 187.1$  kHz. The quality factors of  $Q_1 = 822 \pm 25$  and  $Q_2 = 516 \pm 24$  were determined from the fits. When applying a constant voltage,  $V_{\text{DC}}$ , the resonant frequencies increased according to  $f_{\text{res}}^2(V_{\text{DC}}) - f_{\text{res}}^2(V_{\text{DC}} = 0) \sim V_{\text{DC}}^2$  dependence, which is associated with the electrostatic pulling of the needle and is valid for relatively small frequency changes.<sup>22,23</sup>

The quality factors of  $Q \sim 10^3$  obtained for the diamond needles are quite low compared to singly clamped resonators of similar size, which usually have  $Q \geq 10^4$ .<sup>7,23</sup> We believe that this is due to high energy losses associated with clamping,<sup>24</sup> since the needles were attached to the tungsten holder with a relatively weak Pt contact using focused-ion-beam-induced deposition (FIBID). It is possible to significantly reduce losses and increase the quality factor by optimizing the fixation process. For example, much better mechanical contact can be achieved by fixing the base of the needle inside the hole in the holder using FIBID, as was reported, e.g., in Ref. 25.

In order to analyze the mechanical characteristics of the needles, we performed a numerical simulation based on the finite-element solution of the linear elastic boundary value problem without damping. The model was based on the equation of motion  $-\rho\omega^2\mathbf{u} = \nabla \cdot \mathbf{S}$ ,<sup>26</sup> where  $\rho = 3510$  kg/m<sup>3</sup> is the density of diamond,  $\omega = 2\pi f$  is the angular frequency,  $\mathbf{u}$  is the displacement vector, and  $\mathbf{S}$  is the stress tensor, which depends on Young modulus  $E$  of the material. A three-dimensional geometric model of the needle was constructed using TEM images. The simulated deformation of the needle for two polarizations of the first eigenmode is shown in Fig. 2(d). The ratio of the eigenfrequencies of the two polarizations was proportional to the aspect ratio of the needle cross section  $\sim 0.6$  determined using TEM and was in agreement with the experimental ratio of resonant frequencies  $f_2/f_1$ . The main parameter of the model was Young modulus,  $E$ , which was chosen so that the eigenfrequencies would match  $f_1$  and  $f_2$ . The obtained value  $E = 1130 \pm 50$  GPa is in good agreement with the literature value of  $\sim 1150$  GPa for single crystal CVD diamond<sup>27</sup> and top-down fabricated diamond resonators.<sup>16</sup> The error in determining  $E$  is related to the error in measuring the dimensions of the needle cross section, which was about 5%.

Field emission experiments have shown that at a relatively small distance  $d$  between the diamond needle apex and the anode, sustained mechanical oscillations of the needle can take place when a DC voltage is applied. Figures 3 and 4 demonstrate representative results for large and small  $d$  values, respectively. Figure 3(b) shows the current-voltage characteristic obtained for  $d = 8$   $\mu\text{m}$ , at which no oscillations were observed. The corresponding dependence in Fowler-Nordheim (FN) coordinates, i.e., as  $\ln(I/V_{\text{DC}}^2)$  vs  $1/V_{\text{DC}}$ , demonstrates a non-linear behavior [Fig. 3(c)], which is well described by the FN equation, taking into account the voltage drop inside the needle

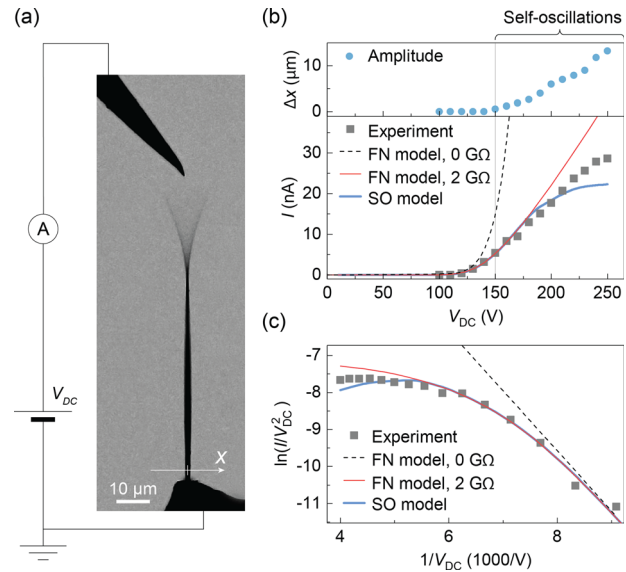


**FIG. 4.** (a) STEM image of the diamond needle during self-oscillation at the anode-cathode distance  $d = 1.3$   $\mu\text{m}$  and  $V_{\text{DC}} = 250$  V. (b) Field emission current-voltage characteristic. Dashed and red lines are fits using Eq. (1) at  $a = 3.1 \times 10^{-8}$  A/V<sup>2</sup>,  $b = 1625$  V,  $R = 0$   $\Omega$ , and  $R = 2$  G $\Omega$ , correspondingly. Blue line is the fit using the self-oscillations model. (c) FN plot for the current-voltage curves shown in panel (b).

$$I = a(V_{\text{DC}} - IR)^2 \exp(-b/(V_{\text{DC}} - IR)), \quad (1)$$

where  $R$  is the resistance of the needle,  $V_{\text{DC}} - IR$  is the voltage at the apex, and  $a$  and  $b$  are the fitting coefficients. At  $R = 0$   $\Omega$ , this equation coincides with the standard FN formula and has the form of a straight line in the FN coordinates shown by the dashed line in Figs. 3(b) and 3(c). At  $R = 2$  G $\Omega$ , the solution of Eq. (1), shown by the red line, gave the best agreement with the experiment.

When the distance  $d$  was reduced to less than 8  $\mu\text{m}$ , mechanical oscillations of the needle were observed at voltages exceeding certain threshold  $V_{\text{thr}}$ . For example, Fig. 4(b) shows the results of field emission measurements at  $d = 1.3$   $\mu\text{m}$ . In this case, oscillations occurred at a voltage higher than  $V_{\text{thr}} = 150$  V. The frequency of oscillations was about 1.4 MHz (see the supplementary material). The amplitude of the needle apex oscillations  $\Delta x$  increased with voltage (and current) [Fig. 4(b)]. The relative deviation of  $\Delta x$  in time from the average value was about 20% at the maximum voltage of 250 V. The current-voltage characteristic shown in Fig. 4(b) was measured with a step of 10 V. At low voltages, the current-voltage curve and the corresponding FN plot are well described using Eq. (1) [red line in Figs. 4(b) and 4(c)]. A significant deviation of the fit from the experimental curve was observed at high voltages due to a strong decrease in the field emission current with the apex-anode distance during oscillations. It is important to note that current-voltage characteristic did not change when the electron beam was blanked. This means that the oscillations are not associated with the action of the electron beam, as, for example, was shown in Ref. 28. Thus, we are dealing with self-oscillations induced solely by a constant DC voltage.

In order to analyze the experimental data, we used the previously developed model of self-oscillations,<sup>11,15,29</sup> based on the equation of motion for a one-dimensional beam  $m^* \ddot{x} = F_{\text{elastic}} + F_{\text{friction}} + F_{\text{Coulomb}}$ . Here,  $m^*$  is the effective mass of the needle and  $x$  is the position of its apex along the horizontal axis, as shown in Fig. 4(a).  $F_{\text{elastic}} = m^* \omega_0^2 x$  is the elastic force (Hooke's law) determined by the fundamental frequency  $f_0 = \omega_0/2\pi$ .  $F_{\text{friction}} = m^* (\omega_0/Q) \dot{x}$  is the friction force, which is linear in velocity and depends on the quality factor  $Q$ .  $F_{\text{Coulomb}} = dW/dx$  is the Coulomb force determined by the electrostatic interaction energy  $W = C(V_0 + V(t))^2/2$ , where  $C$  is the mutual capacitance of the needle and the anode, and  $V_0$  and  $V(t)$  are the DC and AC components of the voltage difference between the needle apex and the anode, correspondingly. The voltages  $V_{\text{DC}}$  and  $V_0 + V(t)$  are related by the Kirchhoff equation  $I_{\text{FN}} + I_c = I_R$  for the equivalent circuit of the system [Fig. 5(a)], where  $I_{\text{FN}}$  is the field emission current,  $I_c = dC(V_0 + V(t))/dt$  is the current through the capacitor, and  $I_R = (V_{\text{DC}} - V_0 - V(t))/R$  is the current through the needle with the resistance  $R$ . An analysis of the motion equation by substituting the solution  $x(t) \sim \cos(\omega_0 t)$  shows that the effective damping coefficient is given by

$$\gamma = \frac{\omega_0}{Q} - \frac{V_0 R \Sigma C}{m^* [1 + (RC\omega_0)^2]} \left( R \Sigma C \frac{\partial I_{\text{FN}}}{\partial x} - C' V_0 \right), \quad (2)$$

where  $R \Sigma = \left( \frac{\partial I_{\text{FN}}}{\partial V} + \frac{1}{R} \right)^{-1}$ . Self-oscillation occurs when the damping becomes negative. Hence, the threshold voltage of self-oscillations  $V_{\text{thr}}$  is determined by the condition  $\gamma = 0$ . The values of the parameters in Eq. (2) were taken from experimental data or calculated by simulation of natural vibrations (similar to how it was done for resonant oscillations) and by electrostatic simulation (see the supplementary material). The values of the fundamental frequency and needle resistance used in the calculations were  $f_0 = \omega_0/2\pi = 1340$  kHz and  $R = 2$  G $\Omega$ . Figure 5(b) shows the calculated  $\gamma(V_{\text{DC}})$  dependences. Since in this case the Q-factor was not measured directly, it was a fitting parameter and was chosen so that the  $V_{\text{thr}}$  matches its experimental value. The best agreement for  $d = 1.3$   $\mu\text{m}$  and  $V_{\text{thr}} = 150$  V was achieved at  $Q = 4500$ , which exceeds Q-factors obtained in resonant excitation experiments. Higher Q-factor can be explained by lower energy losses due to

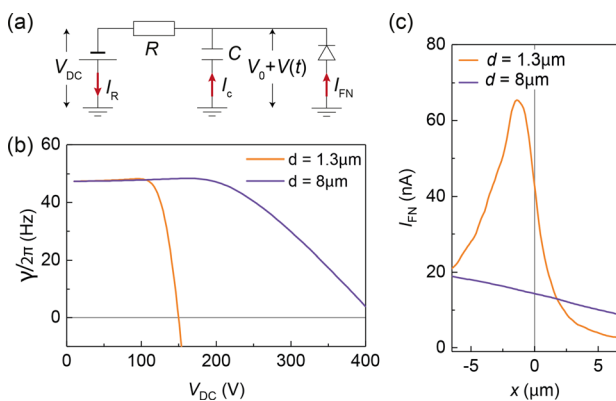


**FIG. 5.** (a) Equivalent electrical circuit of a self-oscillating system. (b) Damping coefficient vs DC voltage calculated using Eq. (2). (c) Field emission current vs the needle apex position calculated at  $V_{\text{DC}} = 250$  V.

clamping, since in this case the size of the Pt contact connecting the needle with the holder was larger compared to the sample shown in Fig. 2(a).

The calculated values of  $V_{\text{thr}}$  increase with the anode–cathode distance  $d$  in accordance with the experiment. For example, Fig. 5(b) shows that at  $d = 8$   $\mu\text{m}$ , damping was positive over the entire voltage range used in the experiment [Fig. 3(b)], i.e., self-oscillation does not take place in this case. The strong dependence of self-oscillations on  $d$  is governed by the parameter  $dI_{\text{FN}}/dx$  in Eq. (2), since the other parameters are almost independent of  $d$ . Figure 5(c) shows the calculated  $I_{\text{FN}}(x)$  dependences. It is clear that  $dI_{\text{FN}}/dx$  at the equilibrium position ( $x = 0$   $\mu\text{m}$ ) is much higher at  $d = 1.3$   $\mu\text{m}$  than at  $d = 8$   $\mu\text{m}$ .

Thus, a simple linear model predicts fairly well the behavior of self-oscillation threshold voltage for a diamond needle. For further comparison with experiment, we used calculated  $I_{\text{FN}}(x)$  dependence to simulate the average current [blue curve in Figs. 4(b) and 4(c)] using the harmonic approximation  $x(t) = \Delta x \sin(\omega_0 t)$ , where  $\Delta x$  is the amplitude given in Fig. 4(b). It can be seen that the simulated  $I(x)$  curve demonstrates strong saturation in the self-oscillation region. The observed quantitative discrepancy between the calculated and experimental  $I(x)$  is expected, since the system is essentially non-linear due to the high oscillation amplitude and the harmonic approximation is not valid.

The above analysis shows that, in general, the properties of diamond needle self-oscillations are similar to those obtained previously for resonators based on carbon nanotubes and SiC nanowires. However, an important difference of the presented experiments is that the anode had the shape of a tip and not a flat surface. As a result, the field emission current is highly dependent on the distance between the apex and the anode, and therefore, the degree of DC to AC conversion is correspondingly higher in this case.

It is also important to note that self-oscillations take place when the period of mechanical oscillations is comparable to the  $RC$  time constant.<sup>11</sup> In the case of self-oscillations presented in Fig. 4, the value of  $RC$  was  $2.2$   $\mu\text{s}$  ( $R = 2$  G $\Omega$ ,  $C = 1.1$  fF) and the period value  $1/\omega_0$  was  $0.12$   $\mu\text{s}$ . Since  $C$  is quite low for high-aspect-ratio emitters, a relatively high  $R$  value is required. As we have recently shown, the Ohmic resistance of diamond needles can be changed from  $\sim 1$  T $\Omega$  for pristine needles to  $\sim 10$  k $\Omega$  for the needles with field-emission-induced graphitization of their surface layer.<sup>18</sup> Hence, in the case of diamond needle emitters, it is possible to adjust the resistance value *in situ* in order to achieve optimal conditions for self-oscillations.

In conclusion, we have shown that the intrinsic mechanical properties of resonators based on singly clamped single-crystal diamond needles mass-produced by CVD are similar to those of diamond resonators fabricated by top-down techniques. It has been established that sustained mechanical oscillations can be induced during field emission from the apex of a diamond needle. This effect is well described by a simple linear model of self-oscillations in a system with a flexible field emitter. In general, the studied diamond needles are very promising for use in various MEMS for sensors, precision measurements, and DC–AC converters, as well as in vacuum microelectronic devices. Moreover, given the nanometer size of the apex, such needles can be used in various scanning probe techniques, for example, as tips for non-contact ultrasensitive force microscopy.<sup>30</sup> It should also be noted

that a promising direction in the study of our diamond needles may be associated with the recently established ability of nanosized diamond structures to undergo ultralarge elastic deformations<sup>31–33</sup> and to change their electrical properties (metallization,<sup>34</sup> superconductivity<sup>35</sup>) under such deformations.

See the [supplementary material](#) for the calculation of the parameters of the self-oscillation model.

We thank Sergey Malykhin for providing SEM images of the diamond needles. The work was supported by Russian Science Foundation (Project No. 19-72-10067).

## AUTHOR DECLARATIONS

### Conflict of Interest

The authors have no conflicts to disclose.

### Author Contributions

**Victor I. Kleshch:** Conceptualization (equal); Funding acquisition (lead); Investigation (lead); Methodology (lead); Supervision (equal); Visualization (lead); Writing – original draft (lead); Writing – review & editing (equal). **Rinat Ramilovich Ismagilov:** Investigation (equal); Writing – review & editing (equal). **Vsevolod V. Mukhin:** Investigation (supporting); Writing – review & editing (supporting). **Anton S. Orekhov:** Investigation (equal); Writing – review & editing (supporting). **Philippe Poncharal:** Investigation (equal); Writing – review & editing (supporting). **Stephen T. Purcell:** Investigation (equal); Supervision (equal); Writing – review & editing (supporting). **Alexander N. Obraztsov:** Conceptualization (equal); Supervision (equal); Writing – review & editing (equal).

### DATA AVAILABILITY

The data that support the findings of this study are available from the corresponding author upon reasonable request.

### REFERENCES

- A. Gaidarzhy, M. Imboden, P. Mohanty, J. Rankin, and B. W. Sheldon, “High quality factor gigahertz frequencies in nanomechanical diamond resonators,” *Appl. Phys. Lett.* **91**, 203503 (2007).
- M. Liao, “Progress in semiconductor diamond photodetectors and MEMS sensors,” *Funct. Diamond* **1**, 29 (2022).
- J. Luo, Y. Q. Fu, H. Le, J. A. Williams, S. Spearing, and W. Milne, “Diamond and diamond-like carbon MEMS,” *J. Micromech. Microeng.* **17**, S147 (2007).
- E. Kohn, P. Gluche, and M. Adamschik, “Diamond MEMS—A new emerging technology,” *Diamond Relat. Mater.* **8**, 934 (1999).
- Y. Tao, J. M. Boss, B. Moores, and C. L. Degen, “Single-crystal diamond nanomechanical resonators with quality factors exceeding one million,” *Nat. Commun.* **5**, 3638 (2014).
- M. J. Burek, D. Ramos, P. Patel, I. W. Frank, and M. Lončar, “Nanomechanical resonant structures in single-crystal diamond,” *Appl. Phys. Lett.* **103**, 131904 (2013).
- P. Ovtarchaiyapong, L. Pascal, B. Myers, P. Lauria, and A. Bleszynski Jayich, “High quality factor single-crystal diamond mechanical resonators,” *Appl. Phys. Lett.* **101**, 163505 (2012).
- A. M. Alexeev, R. R. Ismagilov, and A. N. Obraztsov, “Structural and morphological peculiarities of needle-like diamond crystallites obtained by chemical vapor deposition,” *Diamond Relat. Mater.* **87**, 261 (2018).
- A. N. Obraztsov, P. G. Kopylov, A. L. Chuvilin, and N. V. Savenko, “Production of single crystal diamond needles by a combination of CVD growth and thermal oxidation,” *Diamond Relat. Mater.* **18**, 1289 (2009).
- A. Ayari, P. Vincent, S. Perisanu, M. Choueib, V. Gouttenoire, M. Bechelany, D. Cornu, and S. T. Purcell, “Self-oscillations in field emission nanowire mechanical resonators: A nanometric dc-ac conversion,” *Nano Lett.* **7**, 2252 (2007).
- T. Barois, S. Perisanu, P. Vincent, S. T. Purcell, and A. Ayari, “Role of fluctuations and nonlinearities on field emission nanomechanical self-oscillators,” *Phys. Rev. B* **88**, 195428 (2013).
- J. A. Weldon, B. Aleman, A. Sussman, W. Gannett, and A. K. Zettl, “Sustained mechanical self-oscillations in carbon nanotubes,” *Nano Lett.* **10**, 1728 (2010).
- V. I. Kleshch, A. N. Obraztsov, and E. D. Obraztsova, “Self-oscillations in an electromechanical system with a field emitter,” *JETP Lett.* **90**, 464 (2009).
- V. I. Kleshch, A. A. Zakhidov, A. N. Obraztsov, E. D. Obraztsova, and R. H. Baughman, “Self-oscillations of carbon nanotube twist-yarn during field emission,” *Phys. Status Solidi B* **246**, 2658 (2009).
- V. I. Kleshch, A. N. Obraztsov, and E. D. Obraztsova, “Electromechanical self-oscillations of carbon nanotube field emitter,” *Carbon* **48**, 3895 (2010).
- X. Shen, K. Wu, H. Sun, L. Sang, Z. Huang, M. Imura, Y. Koide, S. Koizumi, and M. Liao, “Temperature dependence of Young’s modulus of single-crystal diamond determined by dynamic resonance,” *Diamond Relat. Mater.* **116**, 108403 (2021).
- V. I. Kleshch, S. T. Purcell, and A. N. Obraztsov, “Single crystal diamond needle as point electron source,” *Sci. Rep.* **6**, 35260 (2016).
- V. I. Kleshch, V. Porshyn, P. Serbun, A. S. Orekhov, R. R. Ismagilov, D. Lützenkirchen-Hecht, and A. N. Obraztsov, “Surface graphitization of diamond nanotips induced by field-emission current,” *Appl. Phys. Lett.* **120**, 141601 (2022).
- A. N. Obraztsov, P. G. Kopylov, B. A. Loginov, M. A. Dolganov, R. R. Ismagilov, and N. V. Savenko, “Single crystal diamond tips for scanning probe microscopy,” *Rev. Sci. Instrum.* **81**, 013703 (2010).
- P. Vincent, P. Poncharal, T. Barois, S. Perisanu, V. Gouttenoire, H. Frachon, A. Lazarus, E. de Langre, E. Minoux, and M. Charles, “Performance of field-emitting resonating carbon nanotubes as radio-frequency demodulators,” *Phys. Rev. B* **83**, 155446 (2011).
- A. Siria, T. Barois, K. Vilella, S. Perisanu, A. Ayari, D. Guillot, S. T. Purcell, and P. Poncharal, “Electron fluctuation induced resonance broadening in nano electromechanical systems: The origin of shear force in vacuum,” *Nano Lett.* **12**, 3551 (2012).
- M. Imboden and P. Mohanty, “Dissipation in nanoelectromechanical systems,” *Phys. Rep.* **534**, 89 (2014).
- S. Perisanu, V. Gouttenoire, P. Vincent, A. Ayari, M. Choueib, M. Bechelany, D. Cornu, and S. Purcell, “Mechanical properties of SiC nanowires determined by scanning electron and field emission microscopies,” *Phys. Rev. B* **77**, 165434 (2008).
- N. Sepulveda, D. Aslam, and J. P. Sullivan, “Polycrystalline diamond MEMS resonator technology for sensor applications,” *Diamond Relat. Mater.* **15**, 398 (2006).
- V. Porshyn, V. I. Kleshch, E. A. Obraztsova, A. L. Chuvilin, D. Lutzenkirchen-Hecht, and A. N. Obraztsov, “Photoinduced effects in field electron emission from diamond needles,” *Appl. Phys. Lett.* **110**, 182101 (2017).
- A. F. Bower, *Applied Mechanics of Solids* (CRC Press, 2009).
- C. A. Klein and G. F. Cardinale, “Young’s modulus and Poisson’s ratio of CVD diamond,” *Diamond Relat. Mater.* **2**, 918 (1993).
- P. Vincent, S. Perisanu, A. Ayari, M. Choueib, V. Gouttenoire, M. Bechelany, A. Brioude, D. Cornu, and S. Purcell, “Driving self-sustained vibrations of nanowires with a constant electron beam,” *Phys. Rev. B* **76**, 085435 (2007).
- A. Lazarus, T. Barois, S. Perisanu, P. Poncharal, P. Manneville, E. De Langre, S. Purcell, P. Vincent, and A. Ayari, “Simple modeling of self-oscillations in nanoelectromechanical systems,” *Appl. Phys. Lett.* **96**, 193114 (2010).

- <sup>30</sup>Y. Tao and C. L. Degen, "Single-crystal diamond nanowire tips for ultrasensitive force microscopy," *Nano Lett.* **15**, 7893 (2015).
- <sup>31</sup>A. Banerjee, D. Bernoulli, H. Zhang, M.-F. Yuen, J. Liu, J. Dong, F. Ding, J. Lu, M. Dao, and W. Zhang, "Ultralarge elastic deformation of nanoscale diamond," *Science* **360**, 300 (2018).
- <sup>32</sup>A. Nie, Y. Bu, P. Li, Y. Zhang, T. Jin, J. Liu, Z. Su, Y. Wang, J. He, and Z. Liu, "Approaching diamond's theoretical elasticity and strength limits," *Nat. Commun.* **10**, 5533 (2019).
- <sup>33</sup>C. Dang, J.-P. Chou, B. Dai, C.-T. Chou, Y. Yang, R. Fan, W. Lin, F. Meng, A. Hu, and J. Zhu, "Achieving large uniform tensile elasticity in microfabricated diamond," *Science* **371**, 76 (2021).
- <sup>34</sup>Z. Shi, M. Dao, E. Tsybalov, A. Shapeev, J. Li, and S. Suresh, "Metallization of diamond," *Proc. Natl. Acad. Sci.* **117**, 24634 (2020).
- <sup>35</sup>C. Liu, X. Song, Q. Li, Y. Ma, and C. Chen, "Superconductivity in compression-shear deformed diamond," *Phys. Rev. Lett.* **124**, 147001 (2020).